CHAPTER 5

Modulation of DNA Repair and the Epigenetic Landscape by Selective Histone Eviction: a Novel Mechanism of Doxorubicin Anti-cancer Activity

Parts of this chapter have been accepted for publication in *Nature Communications*.

ABSTRACT

Induction of DNA damage in tumors is a common strategy in cancer treatment. A major class of chemotherapeutics targets topoisomerase II to induce DNA double-strand breaks resulting in cancer cell death. We considered four members of this class –the anthracyclines doxorubicin, daunorubicin and aclarubicin, the latter of which does not induce DNA breaks–and a chemically unrelated compound, etoposide. We define a unique activity for the anthracyclines: histone eviction from open chromosomal areas by the anti-cancer drugs themselves. As histone variant H2AX, a critical component in the DNA damage response, is also evicted, DNA damage repair is attenuated. Histone eviction affects the epigenetic code and deregulates the transcriptome in tissue culture cells and organs such as the heart. This was confirmed in acute myeloid leukemia (AML) patient samples. Primary AML cells exposed to anthracyclines die due to histone eviction but not by DNA damage, as we showed using drugs that separate these activities. Collectively, we demonstrate that doxo- and daunorubicin combine the activities of two anti-cancer drugs: etoposide for DNA breaks and aclarubicin for histone eviction and epigenetic manipulation. The anthracyclines sense open chromatin and thus transcriptional activity, which may explain their therapeutic window for cancer cells. By studying conventional anti-cancer drugs with new technologies, we define novel mechanism of action and effects of doxo- and daunorubicin on chromatin biology with profound consequences for DNA repair, epigenetics, transcription and anti-cancer activities.

5

Baoxu Pang[1,7], Xiaohang Qiao[1,7], Lennert Janssen[1], Arno Velds[2], Tom Groothuis[1], Ron Kerkhoven[2], Marja Nieuwland[2], Huib Ovaa[1], Sven Rottenberg[3], Olaf van Tellingen[4], Jeroen Janssen[6], Peter Huijgens[6], Wilbert Zwart[5] and Jacques Neefjes[1]*

[1]Division of Cell Biology, [2]Central Genomic Facility, [3]Division of Molecular Biology, [4]Division of Diagnostic Oncology, [5]Division of Molecular Pathology, The Netherlands Cancer Institute, Amsterdam, The Netherlands.
[6]Department of Hematology, VU University Medical Center, Amsterdam, The Netherlands.
[7]These authors contributed equally to this work.
*Correspondence: J. Neefjes, Email: :J.NEEFJES@NKI.NL

INTRODUCTION

In recent years, many critical signaling pathways that drive cancer have been identified, and multiple therapeutic agents designed to target these pathways have demonstrated varying success in cancer treatment[1-4]. Although such agents tend to present fewer side effects compared to conventional anti-cancer drugs, tumor resistance to them is usually swift and constitutes a key limitation. As a consequence, despite the frequently associated adverse effects, the concept of systemic conventional chemotherapy –treating cancer immediately and aggressively– remains standard practice in cancer treatment, especially for aggressive tumors like acute myeloid leukemia (AML). In addition, modern anti-cancer treatment increasingly consists of conventional chemotherapeutic drugs combined with more recently developed targeted anti-cancer drugs.

Doxorubicin (Doxo; also termed Adriamycin®) is one of these "older" conventional drugs[5]. Doxo is widely used in the clinic as a first-choice anti-cancer drug for many tumors and still remains one of the most effective anti-cancer drugs ever developed[6,7]. Millions of cancer patients have been treated with Doxo, or its variant anthracyclines daunorubicin (Daun) or idarubicin (Ida)[8]. These drugs are also included in some 500 reported trials world-wide to explore new and better combinations[9]. The major mechanism of Doxo is believed to be the inhibition of DNA topoisomerase II (TopoII) which induces DNA double-strand breaks[10]. In response to double-strand DNA breaks, cells initiate a canonical repair program that detects the sites of damage and activates the DNA damage response (DDR) signaling cascade to guide recruitment of the repair machinery[11]. If this repair fails, the DDR program initiates apoptosis[11]. Rapidly replicating cells such as tumor cells are presumed to exhibit greater sensitivity to the resulting DNA damage than normal cells, thus constituting a chemotherapeutic window. Other TopoII inhibitors have also been developed and used, including the Doxo analogues Daun, Ida, epirubicin and aclarubicin (Acla) and structurally unrelated drugs such as etoposide (Etop) (Fig. 1a). Etop also traps TopoII after transient DNA double-strand break formation, whilst Acla inhibits TopoII prior to DNA breakage[10]. Exposure to these drugs releases TopoIIα from nucleoli, enabling its accumulation on chromatin (Supplementary Fig. 1). Although these drugs are supposed to have an identical mechanism of action, Etop has fewer long-term side effects than Doxo and Daun, but suffers from a narrower anti-tumor spectrum and weaker anti-cancer efficiency[6], while the overall properties of Acla remain undefined due to its limited use. Despite its clinical efficacy, application of Doxo/Daun in oncology is limited by adverse effects, particularly cardiotoxicity, the underlying mechanism of which is not fully understood[12].

Although the target of the anthracyclines and Etop is TopoII, as identified many decades ago[13,14], this does not exclude additional mechanisms of action. These drugs do have different biological effects which suggest differences in action.

Defining these is important as they may explain effects and side effects of the drugs and support their rational use in (combination) therapies.

Here, we apply modern technologies on an "old" but broadly used drug to characterize new activities and their consequences for cells and patients. We integrate biophysics, biochemistry and pathology with next generation sequencing and genome-wide analyses in experiments employing different anti-cancer drugs with partially overlapping effects. These uncover a novel mechanism of action for the anthracyclines Doxo, Daun and Acla. These drugs induce nucleosome dissociation and evict histones from open chromatin regions. This novel activity leads to modified epigenetic, transcriptional and DNA repair processes and is essential for apoptosis of primary AML blasts. The novel activity of the anthracyclines will have major implications and consequences for anti-cancer treatment with combinations of drugs.

RESULTS

Doxo induces histone eviction in live cells

We have observed loss of histone ubiquitination by proteasome inhibitors[15] and Doxo, without the initiation of apoptosis. While proteasome inhibitors altered the ubiquitin equilibrium, no such effect was detected for Doxo (data not shown). We next tested whether loss of histone ubiquitination may in fact represent loss of histones and examined the effect of Doxo and other TopoII inhibitors on histone stability in living cells.

Importantly, to probe the molecular mechanisms underlying the more potent anti-cancer effects of Doxo, we aimed at mimicking the clinical situation in our experimental conditions. In standard therapy, Doxo and Etop have distinct peak plasma concentrations, which can vary depending on administration schedule with respect to dose, bolus or continuous infusion. In our experiments, we exposed cells to empirical peak-plasma levels of 9μM Doxo or 60μM Etop in accordance with standard therapy [16-19] and analyzed samples after 2 or 4 hrs. Alternatively, cells were further cultured for analysis after drugs were removed with extensive washing after 2 hr exposure. The majority of treated cells endured this treatment when assayed 24 hrs after drug removal (Supplementary Fig. 2).

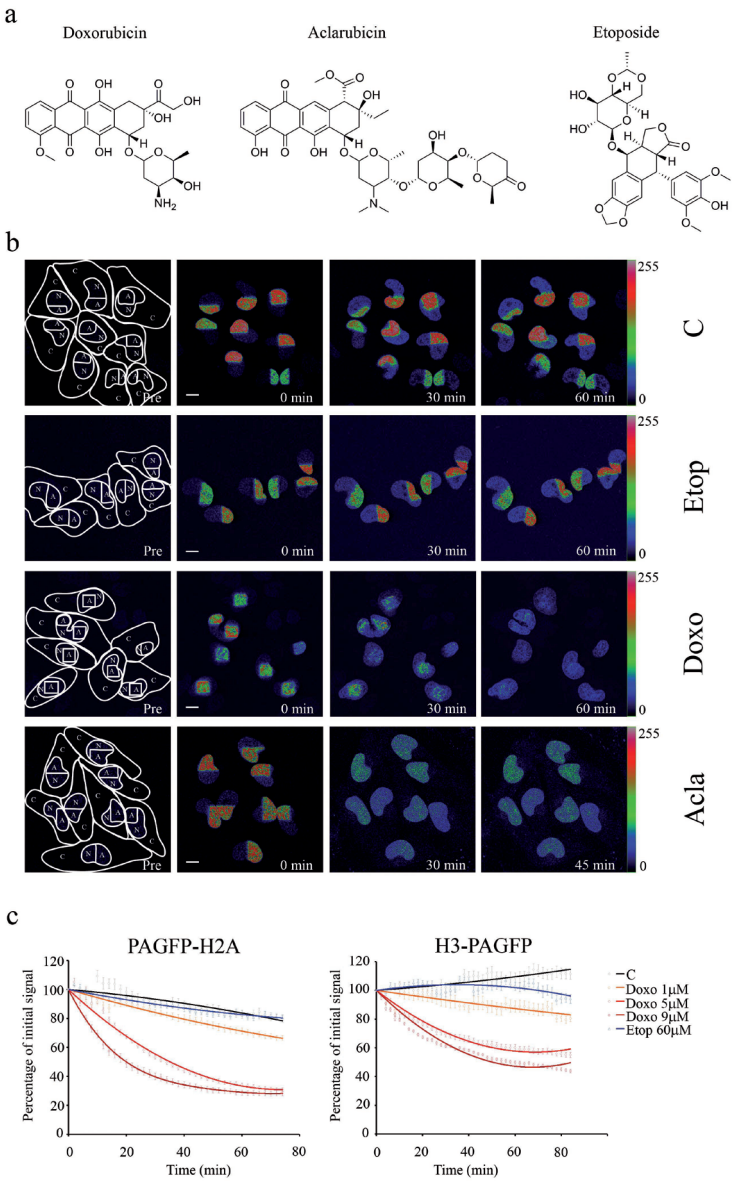

Figure 1. Histone eviction by Doxo. (a) Chemical structures of three TopoII inhibitors doxorubicin, its variant aclarubicin and the structure of etoposide. **(b)** Part of the nucleus from MelJuSo cells expressing PAGFP-H2A was photoactivated. The cells were exposed to 9µM Doxo, 60µM Etop or 20µM Acla for the times indicated and the fate of PAGFP-H2A was monitored by CLSM. The lines in the left panel show the cell boundaries (C), the nucleus (N) and the activated area (A). The fluorescence intensities are shown in false colors as indicated by the 'Look-Up Table'. C, untreated control. Scale bar, 10µm. **(c)** Quantification of the fluorescence in the photo-activated area of MelJuSo cells expressing PAGFP-H2A or H3-PAGFP after exposure to Etop or different concentrations of Doxo. Cells were monitored as in Figure 1b. Mean +/- S.E.M, n=30 to 50 cells. Trend lines are drawn over experimental data.

To probe the stability of histones, different histone variants coupled to photo-activatable GFP (PAGFP) were expressed in the human melanoma cell line MelJuSo. Defined regions of nuclei were photoactivated by 405nm laser light and the fate of the newly fluorescent histone pool was monitored following Doxo, Etop or Acla exposure by confocal laser scanning microscopy (CLSM). Histone PAGFP-H2A was stably integrated into the chromatin of control cells as well as those treated with Etop, but was released when exposed to Doxo or Acla (Fig. 1b; quantification at Supplementary Fig. 3a). The anthracyclines Daun and Ida showed similar results, which suggests that histone release from chromatin represents a more general property of anthracyclines (Supplementary Movies 1-6). These results also imply that histone eviction is independent of TopoII inhibition (since Etop does not evict histones; further confirmed by silencing TopoIIα prior to Doxo exposure, Supplementary Fig. 4), DNA double-strand break formation (which is not observed with Acla; Fig. 3d) or apoptosis (Supplementary Fig. 3c). Histone-eviction resulting from anthracycline exposure was confirmed for histone H3- and H4-PAGFP (Fig. 1c and Supplementary Fig. 3d). The eviction of photoactivated histone variants by Doxo was dose- and time-dependent, and some 30% of histones were released from the activated region (Fig. 1c). Of note, the fates of H2A/H2B and H3/H4 differed following eviction from chromatin, as liberated H2A and H2B were relatively stable and mobile (as detected by FRAP in Supplementary Fig. 3b) in the nucleoplasm, while significant portions of H3 and H4 were destroyed (Supplementary Fig. 3d and e). Doxo and Acla also evicted endogenous H2A from chromatin as free histones were only detected in the soluble fraction of cells exposed to these drugs (Supplementary Fig. 5).

Doxo induces histone eviction from reconstituted nucleosomes *in vitro*

Such dramatic histone eviction has not been previously observed. How then do Doxo and Acla evict histones? To address this, we silenced a series of chromatin modifiers (listed in Supplementary Table 1) by siRNA, but were unable to quench Doxo-mediated histone eviction (data not shown). Histone eviction may also result from intercalation of the anthracyclines Doxo (or Acla) into particular chromatin structures independent of active processes. Since Doxo uptake and accumulation require ATP (Supplementary Fig. 6), MelJuSo/PAGFP-H2A cells were permeabilized with Triton X-100 to remove soluble material from chromatin prior to Doxo treatment, thus stalling ATP-dependent processes (Supplementary Fig. 7). At the same time, the cellular membrane barrier was compromised allowing direct access of drugs to chromatin. Next, half of the nucleus of permeabilized MelJuSo/PAGFP-H2A cells was photoactivated before exposure to drugs, and the fate of fluorescent histones was monitored. Doxo and Acla still induced histone eviction under these conditions (Fig. 2a; quantification in Supplementary Fig. 8), suggesting that ATP-dependent active machinery is not required for histone eviction. Histone eviction is specific to DNA intercalation of anthracyclines, as Etop and ethidium bromide (EtBr) failed to evict histones (Supplementary Fig. 9). Anthracyclines consist of a common tetracycline ring and one or multiple amino sugars. The structure of Doxo

in the DNA double helix shows that the amino sugar makes many interactions with DNA bases in the DNA minor groove[20]. The aglycan form of Doxo, doxorubicinone (Doxo-none) failed to evict histones from permeabilized cells (Fig. 2a), indicating that the amino sugar is critical for histone eviction.

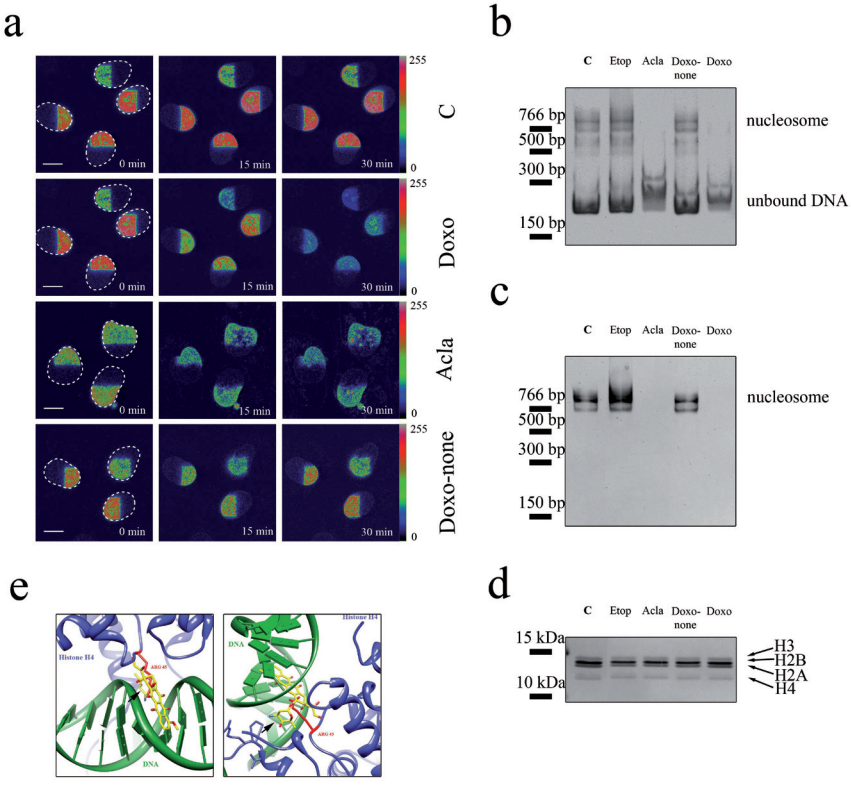

Figure 2. Intercalation of Doxo into DNA suffices to induce histone eviction from nucleosomes. **(a)** MelJuSo cells expressing PAGFP-H2A were permeabilized by 0.1% Triton X-100 before parts of the nucleus were photoactivated by 405nm light. The photoactivated nuclei were followed in time by CLSM prior to or after exposure to 9μM Doxo, 20μM Acla or 20μM Doxorubicinone (Doxo-none), as indicated. Fluorescence intensities shown in false colors and the boundaries of the nuclei are indicated. C, untreated control. Scale bar, 10μm. **(b)** *In vitro* assembled single nucleosomes were treated with 60μM Etop, 20μM Doxo, 20μM Acla or 20μM Doxorubicinone for 4 hrs as indicated. C, untreated control. Samples were analyzed by native PAGE and stained with ethidium bromide (EtBr). Position of assembled nucleosomes and free DNA are indicated. **(c)** The same gel in (b) was subsequently stained with silver to visualize the histones in the nucleosomes. Position of assembled nucleosomes is indicated. **(d)** The same samples as in (b) and (c) were analyzed by SDS-PAGE and silver-stained to show that equal amounts of histones and reconstituted single nucleosomes were present in the different lanes. Positions of histone variants are indicated. **(e)** A model of Doxo intercalation in chromatin with the sugar moiety of Doxo competing with H4 amino acids for access to space in the DNA minor groove. Doxo has been co-crystallized with a segment of the DNA double helix (PDB: 1D12). The nucleosome structure has been crystallized (PDB:1AOI) but without Doxo. Doxo, based on the Doxo-DNA structure, was docked into the nucleosome structure (using program UCSF Chimera). Shown is a snapshot of the relevant area of the Doxo-chromatin model under two angles. DNA is visualized in green, Doxo in yellow, histone H4 in blue and the H4 Arginine residue (at position 45) that enters the DNA minor groove is shown in red. The

amino-sugar of Doxo (shown by arrow) also fills the DNA minor groove and makes various interactions with DNA bases.

Even in permeabilized systems, an additional contribution of proteins cannot be excluded. We therefore reconstituted single nucleosomes from purified recombinant histones and DNA, before exposure to the various drugs. Intact reconstituted single nucleosomes migrated slower than the free DNA on native gels, as detected either by ethidium bromide staining for DNA (Fig. 2b) or by silver staining for histones (Fig. 2c). Doxo and Acla (unlike Etop or Doxo-none) dissociated nucleosomes in this *in vitro* setting. The dissociated histones were not visible under native conditions as they are basic and have a charge opposite of DNA and moved from the native gel to the negative pole. However, equal amounts of input nucleosomes/histones could still be visualized when the same samples were analyzed under fully denaturing conditions (Fig. 2d). This *in vitro* reconstituted system unambiguously demonstrates that the chemical structures of Doxo or Acla suffice to dissociate nucleosomes for histone release.

In order to understand the molecular mechanism of histone eviction induced by Doxo and Acla, we combined the separate structures of DNA-Doxo[20] and nucleosomes[21] to model how Doxo may affect nucleosome structure (Fig. 2e). The model predicts that Doxo, especially its amino sugar group, competes for space with the H4-Arginine residue in the DNA minor groove, which is critical for the stabilization of nucleosome structures[21]. Acla also has a bulky moiety that contains three sugars attached to the tetracycline ring and could share the same mechanism of histone eviction. As the aglycan form of Doxo does not evict histones and histone eviction proceeds independently of ATP, the model suggests that incorporation of the Doxo tetracycline ring into the DNA double helix structure positions the amino sugar in the DNA minor groove to efficiently compete for space with residues of histones important for nucleosome stabilization. When the amino-sugar occupies this space, chromatin destabilization will be the consequence.

Doxo-induced histone eviction impairs DNA damage response

An early response to DNA double-strand breaks is the phosphorylation of histone variant H2AX by ATM kinase, which is essential for the propagation of downstream DNA damage response (DDR) signals from damaged sites[11]. Consequently, phosphorylated H2AX (γ-H2AX) is used as a node for active DDR[22]. If Doxo combines local H2AX eviction with DNA damage, the ensuing repair may be negatively affected. We tested whether Doxo also evicts H2AX by assaying photoactivated PAGFP-H2AX in MelJuSo cells. The PAGFP modification of H2AX did not affect its phosphorylation in response to Etop (Supplementary Fig. 10) and PAGFP-H2AX was also evicted by Doxo (Fig. 3a; quantification in Supplementary Fig. 11). We further compared endogenous γ-H2AX formation in MelJuSo cells exposed to Doxo or Etop. γ-H2AX was strongly induced by Etop but considerably less by Doxo (Fig.

3b and c), even at concentrations yielding similar levels of DNA double-strand breaks (Fig. 3d). Since γ-H2AX acts as a node in DDR, factors acting downstream, such as MDC1[23], also showed poor staining in Doxo but high in Etop-exposed cells (Supplementary Fig. 12). This attenuation of γ-H2AX formation is not due to general DDR pathway inhibition (Supplementary Fig. 13), but may result from H2AX eviction that then cannot be phosphorylated by ATM at the DNA breaks. Consequently, downstream events such as phosphorylation of ATM substrates, feedback signaling pathways including phosphorylation of MRE11 [24] (Supplementary Fig. 14) and ultimately overall DDR were attenuated following Doxo exposure.

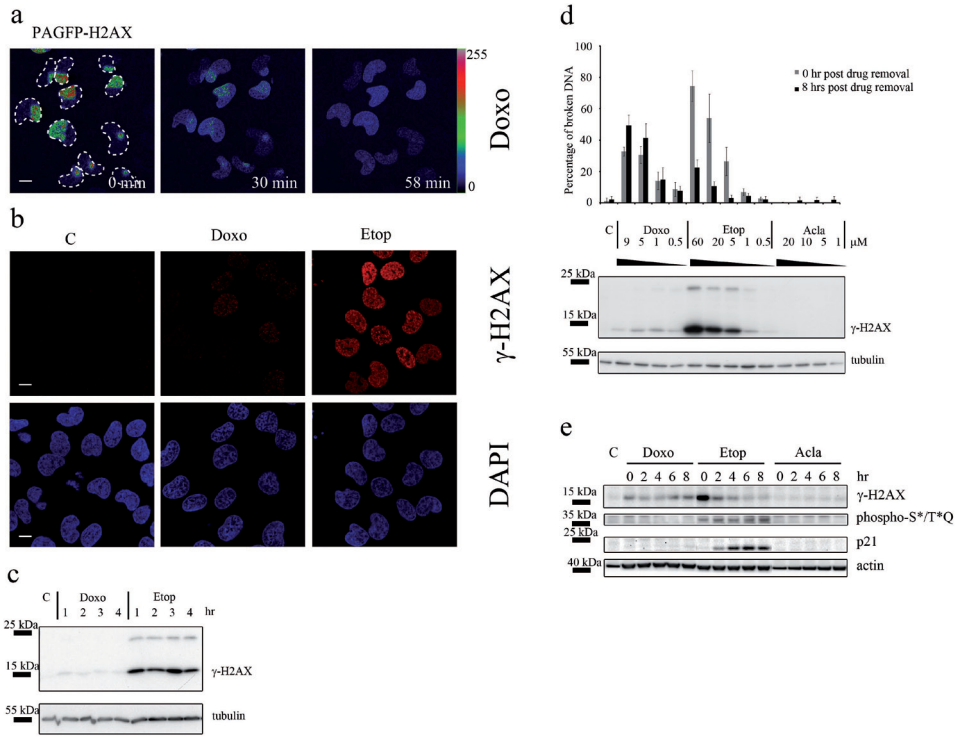

Figure 3. Doxo induces H2AX eviction and attenuates DNA damage response. (a) Part of the nucleus of MelJuSo cells expressing PAGFP-H2AX was activated before exposure to Doxo. The boundaries of nuclei are indicated. Fluorescence intensities are shown in false colors. Scale bar, 10μm. **(b)** MelJuSo cells were treated with 9μM Doxo or 60μM Etop for 2 hrs before fixation and stained for γ-H2AX (top panel: in red). Bottom panel in blue indicates DAPI staining of the nuclei of cells. C, untreated control. Scale bar, 10μm. **(c)** MelJuSo cells were treated with 9μM Doxo or 60μM Etop and lysed at indicated time points before analyses of γ-H2AX by SDS-PAGE and western blotting. Tubulin is used as a loading control and the positions of molecular weight markers are indicated. **(d)** MelJuSo cells were exposed to various concentrations of Doxo, Etop or Acla for 2 hrs. C, untreated control. Drugs were removed by extensive washing. DNA double-strand breaks, immediately after 2 hrs drug treatment or 8 hrs post drug removal were quantified by constant-field gel electrophoresis and expressed as percentage of total DNA (mean +/- SD, n=3 of independent experiments). Western blot indicates the γ-H2AX response after 2 hrs drug treatment at different concentrations; tubulin is shown as loading control. **(e)** MelJuSo cells were exposed to 9μM Doxo, 60μM Etop or 20μM Acla for 2 hrs. Drugs were removed and further cultured for

the times indicated. Cells were lysed, separated by SDS-PAGE and WB was probed with the antibodies indicated. Actin is used as loading control and positions of marker are indicated. C, untreated control.

We directly visualized the consequences of Doxo, Etop or Acla on DNA repair by constant-field gel electrophoresis used to quantify DNA double-strand breaks[25] (Fig. 3d). Unlike Acla, Etop effectively induced DNA breaks at 2 hrs after drug exposure followed by efficient repair by 8 hrs after drug removal. Conversely, DNA repair failed after Doxo removal (Fig. 3d), as also observed before[26], though Doxo was excreted efficiently from the treated cells (Supplementary Fig. 15). Proper DDR after Etop removal was also deduced from rapidly decreased γ-H2AX staining, whereas γ-H2AX persisted in Doxo-exposed cells indicating un-repaired DNA damage (Fig. 3e). The delayed onset of secondary effects following Doxo removal included delayed p21 expression and attenuated ATM/ATR activation as monitored by substrate phosphorylation (Fig. 3e). The progression into the G2/M cell cycle check point and the subsequent arrest that is usually induced by DNA double-stand breaks were also delayed (Supplementary Fig. 16). Collectively, these observations illustrate that the TopoII inhibitors Doxo and Etop both generate DNA double-strand breaks, yet differ in solving this problem. The new effect of Doxo on histone eviction and the subsequent impairment of the DDR signaling could be one of the contributors that lead to the defect of DNA damage repair during Doxo treatment.

Mitotic cells resist Doxo-induced histone eviction and attenuated DDR

Since not all histones were evicted by Doxo and Acla (Fig. 1), we reasoned that anthracyclines may show a preference for particular chromatin structures. This became apparent when detecting a few Doxo-exposed MelJuSo cells that stained strongly for γ-H2AX compared to the vast majority in the same culture (Fig. 4a, left). DAPI staining indicated that these cells were in prophase or early phase of mitosis when chromatin is in a more condensed state (Fig. 4a, right; also shown for mitotic cells in Supplementary Fig. 17). To enrich for these, cells were arrested in mitosis by 6 hr exposure to nocodazole. Mitotic cells were isolated by a mild shake-off and responses to Doxo or Etop (added for 1 or 2 hrs) were determined by staining cell lysates with anti-γ-H2AX antibodies. Doxo-treated mitotic (floating) cells exhibited a strong γ-H2AX response that is comparable to Etop (Fig. 4b). To visualize histone dynamics during mitosis, nocodazole-enriched mitotic or non-mitotic MelJuSo/PAGFP-H2A cells were exposed to Doxo following photoactivation of a portion of chromosomal material. Cells were analyzed 2 hrs later for the distribution of fluorescent PAGFP-H2A and Doxo (Doxo is red fluorescent and stains DNA). Whilst activated fluorescent histones were evicted in interphase cells now occupying the entire nuclear space (Fig. 4c, bottom panel), they remained sequestered to a subset of condensed chromosomes in mitotic cells (Fig. 4c, top panel). Doxo enters condensed chromatin during mitosis but fails to evict histones for the redistribution over the other chromosomes outside the field of photoactivation and gives proper

DNA damage responses. This also suggests that Doxo has certain specificity for the type of chromatin where histone eviction occurs.

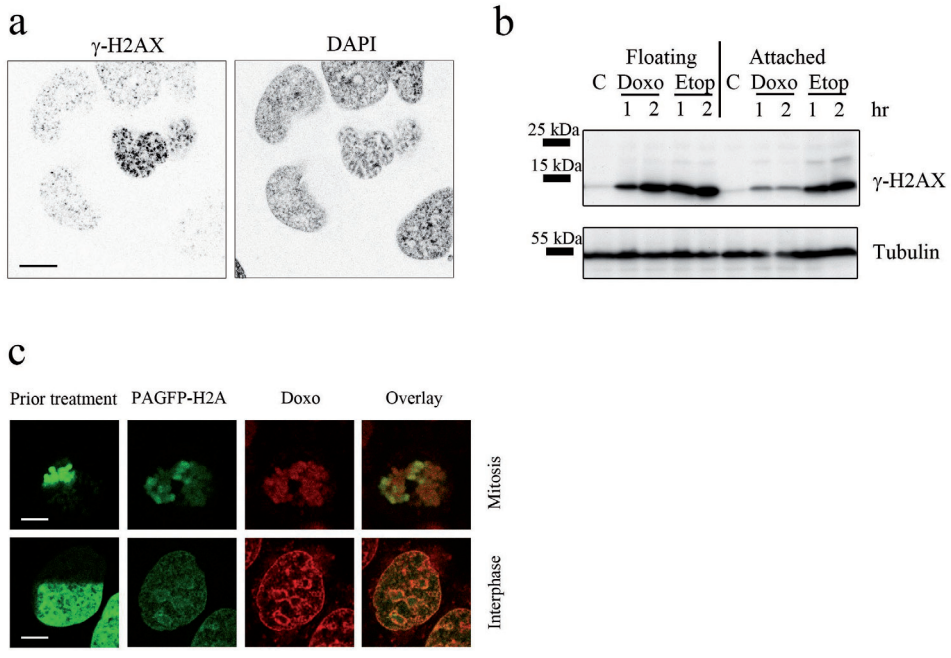

Figure 4. Mitotic cells resist Doxo-induced histone eviction and allow DNA damage responses. **(a)** MelJuSo cells were exposed to 9μM Doxo for 2 hrs before fixation and stained for γ-H2AX and with DAPI. Scale bar, 10μm. **(b)** MelJuSo cells were cultured for 6 hrs in the presence of nocodazole to accumulate mitotic cells before additional exposure for 1 or 2 hrs to 9μM Doxo, 60μM Etop or control ('C'). Floating cells (mainly mitotic cells) and attached (non-mitotic) cells were collected from the same culture and analyzed by SDS-PAGE and WB. The filter was probed for γ-H2AX and tubulin was used as loading control. Positions of marker proteins are indicated. **(c)** MelJuSo cells expressing PAGFP-H2A were pre-treated with nocodazole for 6 hrs. Part of the nucleus of a mitotic (top panel) or interphase cell (bottom panel) was photoactivated (left) followed by 9μM Doxo exposure for another 1 hr. Green color represents photoactivated histone H2A. Red color visualizes Doxo intercalated into chromatin. Scale bar, 10μm.

Doxo alters the transcriptome

Histones carry different epigenetic modifications and these chromatin marks can be lost by eviction during Doxo treatment. After drug removal (or clearance from the patient's circulation), the evicted histones may reintegrate into chromatin (Supplementary Fig. 18) or be replaced by newly synthesized histones. This would affect the epigenetic code associated with these histones and then affect the transcriptome. To test this, MelJuSo cells were exposed for 2 hrs to Doxo, Etop or Acla. After drug removal and extensive washing, cells were cultured for 24 hrs or 6 days prior to RNA extraction for microarray analysis. Acla was included for the effects of histone eviction without DNA damage, and Etop for DNA damage without

histone eviction. Quantifying the number of transcripts that were differentially expressed by at least a factor of 2 relative to untreated cells indicated that Doxo- and Acla-exposure exhibited strong effects on the transcriptome (Fig. 5a and Supplementary Fig. 19a). More than twice the number of differentially expressed genes was observed 1 day following treatment with Doxo or Acla as compared to Etop, despite the stronger initial DNA damage and DDR signaling produced by the latter (Fig. 3d). Similar results were also observed for the human colon cancer cell line SW620 (Fig. 5a and Supplementary Fig. 19a). To test whether Doxo always affects the same set of genes, the analyses were independently repeated with MelJuSo cells. The same set of genes was differentially regulated after Doxo exposure, suggesting specific effects of Doxo on the transcriptome of cells (Supplementary Fig. 19). The genes differentially expressed in MelJuSo cells 1 day after exposure to the drugs were analyzed by Ingenuity Pathway Analysis. Etop showed a strong enrichment for genes in the DNA damage response, while other pathways were selectively affected by Doxo and Acla (Supplementary Table 2). Though Doxo and Etop both inhibit TopoII for DNA double-strand break formation, they affect different pathways in cells. This may be due to the new activity of Doxo on histone eviction. The transcriptional differences between Doxo and Acla may result from additional effects on DNA double-strand breaks following Doxo exposure or different regions of histone eviction induced by these two drugs.

Selectivity of Doxo-induced histone eviction at open-chromatin regions

As chromatin has different conformational states[27,28], we wondered whether Doxo would show any selectivity in histone eviction. We analyzed multiple histone markers in the chromatin fraction exposed to the drugs for 4 hrs (Fig. 5b and Supplementary Fig. 20). Doxo treatment decreased histones marked by H3K4me3 (found around active promoter regions)[28] that represent open transcriptionally active chromatin structures. By contrast, no reduction of H3K27me3 in chromatin was observed (Fig. 5b). H3K27me3 usually associates with inactive/poised promoters and polycomb-repressed regions, and correlates with compact chromatin[28]. These data suggest that histones are evicted from particular chromatin regions by Doxo. Yet, Doxo also reduces H3K9me3 that usually specifies repressed regions[29], implying that the specificity of Doxo-mediated histone eviction is not restricted to open chromatin only.

To define preferred regions of histone eviction by Doxo and Acla in a genome-wide fashion and at a higher resolution, we performed formaldehyde-assisted isolation of regulatory elements coupled to next-generation sequencing (FAIRE-seq) on MelJuSo cells treated with Doxo, Acla or Etop for 4 hrs to identify histone-free DNA[30,31]. After formaldehyde fixation of histone-DNA interactions and mechanical DNA breakage, the chromatin was exposed to a classical phenol-chloroform extraction to achieve accumulation of histone-free DNA in the aqueous phase while

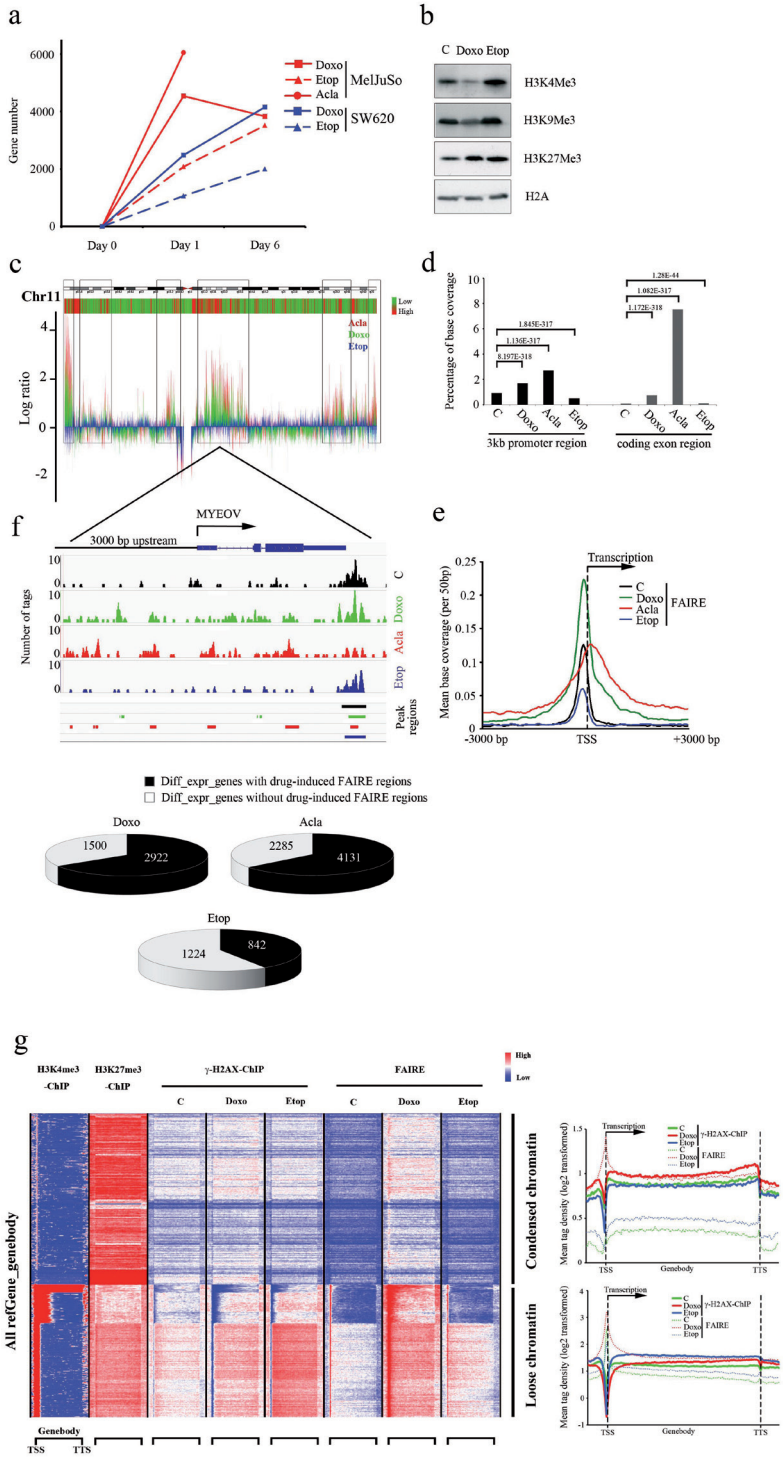
a
Gene number
6000
4000
2000
0
Day 0
Day 1
Day 6
Doxo
Etop
Acla
MelJuSo
Doxo
Etop
SW620
b
C Doxo Etop
H3K4Me3
H3K9Me3
H3K27Me3
H2A
c
Chr11
Low
High
Acla
Doxo
Etop
Log ratio
4
2
0
-2
d
Percentage of base coverage
1.29E-44
1.082E-317
1.172E-318
1.845E-317
1.136E-317
8.197E-318
C
Doxo
Acla
Etop
3kb promoter region
coding exon region
e
Transcription
Mean base coverage (per 50bp)
0.25
0.2
0.15
0.1
0.05
0
C
Doxo
Acla
Etop
FAIRE
-3000 bp
TSS
+3000 bp
f
MYEOV
3000 bp upstream
Number of tags
C
Doxo
Acla
Etop
Peak regions
Diff_expr_genes with drug-induced FAIRE regions
Diff_expr_genes without drug-induced FAIRE regions
Doxo
1500
2922
Acla
2285
4131
Etop
1224
842
g
H3K4me3 -ChIP
H3K27me3 -ChIP
γ-H2AX-ChIP
FAIRE
C
Doxo
Etop
High
Low
All refGene_genebody
Genebody
TSS
TTS
Condensed chromatin
Loose chromatin
Mean tag density (log2 transformed)
Transcription
γ-H2AX-ChIP
FAIRE

Figure 5. Selective histone eviction and transcriptome changes by Doxo and Acla. (a) MelJuSo or SW620 cells were exposed to 9μM Doxo, 10μM Acla or 60μM Etop for 2 hrs. The drugs were removed and cells were cultured for 24 hrs or 6 days. Line was discontinued after day one after Acla exposure due to apoptosis later during culture. Microarray analyses were performed for all samples. Plotted are the genes with more than 2-fold difference in expression compared to non-treated cells. **(b)** Endogenous histone modification changes by Doxo. MelJuSo cells were treated with 9μM Doxo or 60μM Etop for 4 hrs. Chromatin was isolated, separated by SDS-PAGE and WB probed with antibodies against the histone modifications indicated. **(c)** MelJuSo cells were exposed to 9μM Doxo, 20μM Acla or 60μM Etop for 4 hrs before histone-free DNA fragments were isolated by FAIRE followed by next generation sequencing. Shown is chromosome 11, with a green-red bar showing the corresponding relative gene-density. The sequenced reads (Acla, red; Doxo, green; Etop, blue) of the different treatments were normalized and compared to control cells. The boxed areas indicate sites more efficiently isolated by FAIRE and their positions in the gene density bar. **(d)** Annotation of FAIRE-seq peak regions. The peak region coverage was enriched in the coding exon and promoter regions compared to control cells, due to anthracycline treatments. *p*-values were calculated with Fisher's exact test. **(e)** Distribution and enrichment of FAIRE regions around TSS. The peak regions from FAIRE-seq were enriched around the TSS for all RefSeq genes. **(f)** Drug-induced peak regions defined by FAIRE-seq after 4 hr Doxo or Acla treatment were compared to the differentially expressed genes in MelJuSo cells 24 hrs after the respective drug exposure (relative to the control cells). This is illustrated for gene MYEOV located on chromosome 11. The FAIRE-seq reads and peak regions called for the different conditions are indicated. Black area in the pie charts defines differentially expressed genes with drug-induced FAIRE peak regions (relative to control cells) within 3 kb upstream of the TSS or on the gene bodies. The new peak regions induced by Doxo and Acla exposure are indicated by arrows. **(g)** Comparison of reads for FAIRE-seq and ChIP-seq of γ-H2AX for all RefSeq gene bodies. Gene bodies are normalized between transcriptional start (TSS) and termination sites (TTS). Active genes in control MelJuSo cells are defined by accumulation of H3K4me3 peak regions around TSS (shorter genes fill larger areas of H3K4me3 due to normalization between TSS and TTS) while inactive genes accumulate H3K27me3, as indicated. Clustering reveals two major classes. A color bar indicates the relative density of the reads. Right panels: Quantification of the γ-H2AX reads from control, Etop or Doxo treated cells over the normalized total gene bodies with TSS and TTS indicated (solid lines). The corresponding FAIRE-seq reads are shown by dotted lines. The data are separated for the transcriptionally-active (bottom) and -inactive (top panel) genes.

histone-bound DNA fragments accumulate in the organic phase[30] (Supplementary Fig. 21). The histone-free DNA fragments in the aqueous phase were subjected to next-generation sequencing. To globally visualize the histone-evicted regions, the sequenced read counts were normalized and compared to those of control cells (Fig. 5c for chromosome 11; Supplementary Fig. 22 for all chromosomes; for statistics of all next-generation sequencing runs, see Supplementary Table 3). Exposing MelJuSo cells to Doxo or Acla induced a marked enrichment of histone-free DNA fragments from particular regions of the chromosome, whilst Etop exposure did not generate additional histone-free DNA fragments. Further annotation of FAIRE-seq peak regions was performed to define these regions and revealed a strong enrichment of promoter and exon regions after Doxo or Acla exposure (Fig. 5d and Supplementary Fig. 23a). Doxo and Acla acted not identical yet very similar (50% overlap in enriched promoter regions, Supplementary Fig. 23b and c).

The FAIRE-seq peak regions that indicate the histone-free DNA were often found around the transcription starting sites (TSS)[30] and these were further enriched by Doxo or Acla treatment (Fig. 5d and e). In addition, the boundaries of the histone-free zones around the TSS were broadened by exposure to Doxo or Acla (Fig. 5e),

suggesting that histone eviction extends beyond the 'open chromatin' structure detected in control or Etop-exposed cells that share similar confined peak-region boundaries. The accessibility of the TSS also correlates to gene activity[30]. Note that Etop reduced the enrichment of FAIRE peak regions around TSS, corresponding to diminished transcription post-drug treatment, while Doxo enhanced both (Fig. 5d and e). The histone eviction induced by Doxo or Acla was not restricted to MelJuSo cells, and could be reproduced in the colon cancer cell line SW620 (Supplementary Fig. 24). There are shared regions enriched in the two different cell lines by the anthracyclines (Supplementary Fig. 24d), indicating the reproducibility of the FAIRE-seq data and that common chromatin structures are targeted for histone eviction.

To test the relationship between histone eviction and transcriptome alterations, as detected by microarray analyses, both data sets from MelJuSo cells were integrated (Fig. 5f). Doxo- or Acla-induced histone eviction and yielded epigenetic changes in promoter regions (defined as 3 kb upstream of the TSS) and gene body regions that would affect transcription of the respective genes directly. Presence of Doxo-induced FAIRE-seq peak regions within 3kb upstream of the TSS or in the gene bodies was detected in 70% of differentially expressed genes altered by Doxo. This was also observed for Acla-treated but not for Etop-treated cells (Fig. 5f, Supplementary Fig. 25), indicating that Doxo and Acla locally affect chromatin structure and epigenetic modifications. This correlates to the altered transcription of the neighboring genes, as exemplified by the MYEOV gene (Fig. 5f; more genes and statistics in Supplementary Fig. 25).

Doxo-induced histone eviction and γ-H2AX abrogation at active genes

If Doxo evicts histones from open chromatin, it should affect DDR in the histone eviction regions whereas it should mimic effects of Etop in more compact chromatin. We performed ChIP-seq experiments, isolating γ-H2AX associated DNA fragments from MelJuSo cells either not treated or treated with Doxo or Etop for 4 hrs. Additional ChIP-seq experiments for H3K4me3 (defining active/weak promoters like loose chromatin structures) and H3K27me3 (defining inactive/poised genes and relative condensed chromatin structures) histone marker in non-treated cells were also performed to define the chromatin state and transcriptional potency for all RefSeq genes. Then all genes were normalized between transcription start site (TSS) and transcription termination site (TTS) and subsequently clustered. These data were paired with γ-H2AX ChIP-seq and FAIRE-seq data for gene bodies at the identical order (Fig. 5g). The (relative) intensities of the read-tags are represented by a color bar. Open and closed chromatin is not only represented by the characteristic histone marks but also distinguished by the FAIRE-seq data. Doxo preferentially evicts histones around the TSS with loose (H3K4me3-containing) chromatin structure. Notably, both Etop and Doxo induced more γ-H2AX in transcriptionally active genes marked by H3K4me3 modification, compared to inactive genes. At inactive genes, the γ-H2AX response to Doxo and Etop is almost identical. A further quantification

of the read-tags in the gene bodies in open and closed chromatin reveals that Doxo strongly decreases or delays DNA damage responses (visualized by fewer γ-H2AX reads) around the TSS and the beginning of the gene body while this effect wanes at the end of genes. The FAIRE-seq reads show an inverse relationship (Fig. 5g, right panels). These data show that Doxo evicts histones from open chromatin and suggests that the DDR response exemplified by γ-H2AX is interrupted due to local histone eviction. DNA damage responses following Doxo or Etop exposure are not equally spread over the chromosome but merely concentrated in transcriptionally active open chromatin where the response to Doxo is attenuated. No such effect was detected in closed chromatin. Thus Doxo may be considered a drug sensing transcriptionally active DNA for histone eviction and attenuated DNA repair.

Histone eviction affects the epigenetic landscape before transcriptionally active genes

Epigenetic modifications on various histones, combined with the genetic information in DNA, control the gene expression and shape the identity of each cell. While more condensed chromatin regions marked by H3K27me3 were resistant to Doxo-induced histone eviction (Fig. 5b for western blot; Supplementary Fig. 26 for H3K27me3 ChIP-seq experiments at different time points), Doxo treatment erases particular histone marks such as histone H3K4me3 that mark active genes and are involved in the regulation of transcription[32] (Fig. 5b), the question is whether these marks would properly re-integrate after Doxo removal. Organizations of histone mark H3K4me3 as well as other local marks occupying the promoter regions of genes determine proper transcription initiation[33], implying that epigenetic changes in these regions could have major effects on the transcriptome of Doxo- and Acla-exposed cells, as we have observed (Fig. 5a). To test whether anthracyclines could affect the epigenetic landscape, MelJuSo cells were collected 0 hr (Supplementary Fig. 27) and 24 hrs (Fig. 6) post drug removal and ChIP-seq experiments were performed with antibodies against histone mark H3K4me3. Etop exposed cells were used as a control for effects due to DNA damage response. When all peak regions from drug-exposed cells were compared and aligned around TSS, a 100 bp shift of peak regions towards the TSS was observed from Doxo-treated cells 24 hrs post drug removal (Fig. 6a, top panel), as well as immediately after drug removal (Supplementary Fig. 27). Furthermore, this shift is towards the FAIRE-seq peak regions, representing sites of histone eviction (Fig. 6a, bottom panel). As Etop did not affect the location of the peak regions, this effect could not be due to DNA breaks or repair. This is further confirmed by the peak regions of Acla-treated cells that also shifted even though Acla does not induce DNA breaks yet evicts histones. This illustrates the power of using different drugs with overlapping effects for deciphering the molecular basis of complicated effects. When the shifted regions of Doxo-exposed cells 0 hr and 24 hrs post drug removal were compared, the majority of them were shared between the two groups (Supplementary Fig. 27h), indicating these epigenetic changes were the result of initial histone eviction and

these changes persisted for at least 24 hrs that could contribute to the deregulated transcription of Doxo-treated cells. It should be noted that Acla exerted a stronger histone-eviction effect and that H3K4me3 ChIP-seq signals were diminished during Acla exposure (Supplementary Fig. 27), whilst 24 hrs after drug removal this histone modification recovered partially, with the reminiscence of shift of peak regions towards the TSS, similar to Doxo treatment.

Further analysis of the H3K4me3 peak regions around the TSS allowed segregation of the data set into two sub-cluster regions: one cluster of regions with the peak shift (Fig. 6b) and one cluster of regions without peak shift after Doxo exposure (Fig. 6c). The regions in the two distinct sub-clusters are not in close vicinity (Fig. 6d), when a 6 kb window centered at TSS was applied. This suggests that Doxo and Acla affect the location of H3K4me3 of defined genes. To define the nature of the two classes of genes, we compared the efficiency of histone eviction by Doxo and Acla on the H3K4me3 marked regions within the two sub-cluster regions (using the FAIRE-seq data) but did not observe obvious differences (Fig. 6e and f). Since histone H3K4me3 modification marks both active and weak promoters[28] and Doxo senses open chromatin, we wondered whether transcription activity could correlate to shifting of the H3K4me3 mark after Doxo or Acla exposure. We compared expression rates of genes within the two sub-clusters. Transcription activity of genes within the sub-cluster where H3K4me3 shifted was significantly higher when compared to the genes with an unaltered location of H3K4me3 (Fig. 6g). This suggests that transcriptional activity of genes is sensed by Doxo and Acla for histone H3K4me3 repositioning, as detected 24 hrs after exposure to Doxo or Acla. Possibly, higher transcription relates to a more open structure of chromatin that may –following Doxo or Acla induced histone eviction– drive sliding of the H3K4me3 mark to about 100 bp closer to the TSS resulting in an altered epigenetic print.

Tissue selective effects of Doxo and histone eviction *in vivo*

A major side effect of Doxo is cardiotoxicity[34]. Since balanced transcription is critical for proper heart function, pathological changes in the heart correlate to deregulation of gene expression and epigenetic changes[35], and persistent DNA damages could also impose cardiotoxicity, we reasoned that histone eviction may also contribute to cardiotoxicity imposed by Doxo. This was tested in mice injected *iv* with 10 mg/kg (≈30 mg/m²) of Doxo or 35 mg/kg (≈105 mg/m²) of Etop. The pharmacokinetics (clearance, half-life and volume of distribution (Vd)) of Doxo in mice[36] and humans[37] display remarkable similarities, supporting the translation of our observations. Doxo may accumulate in tissues resulting in levels of about 20μM in liver, heart and lung 1 hr after *iv* injection[36]. As Acla is an infrequently used anti-cancer drug with poorly understood pharmacokinetics in mice, this drug was not further included.

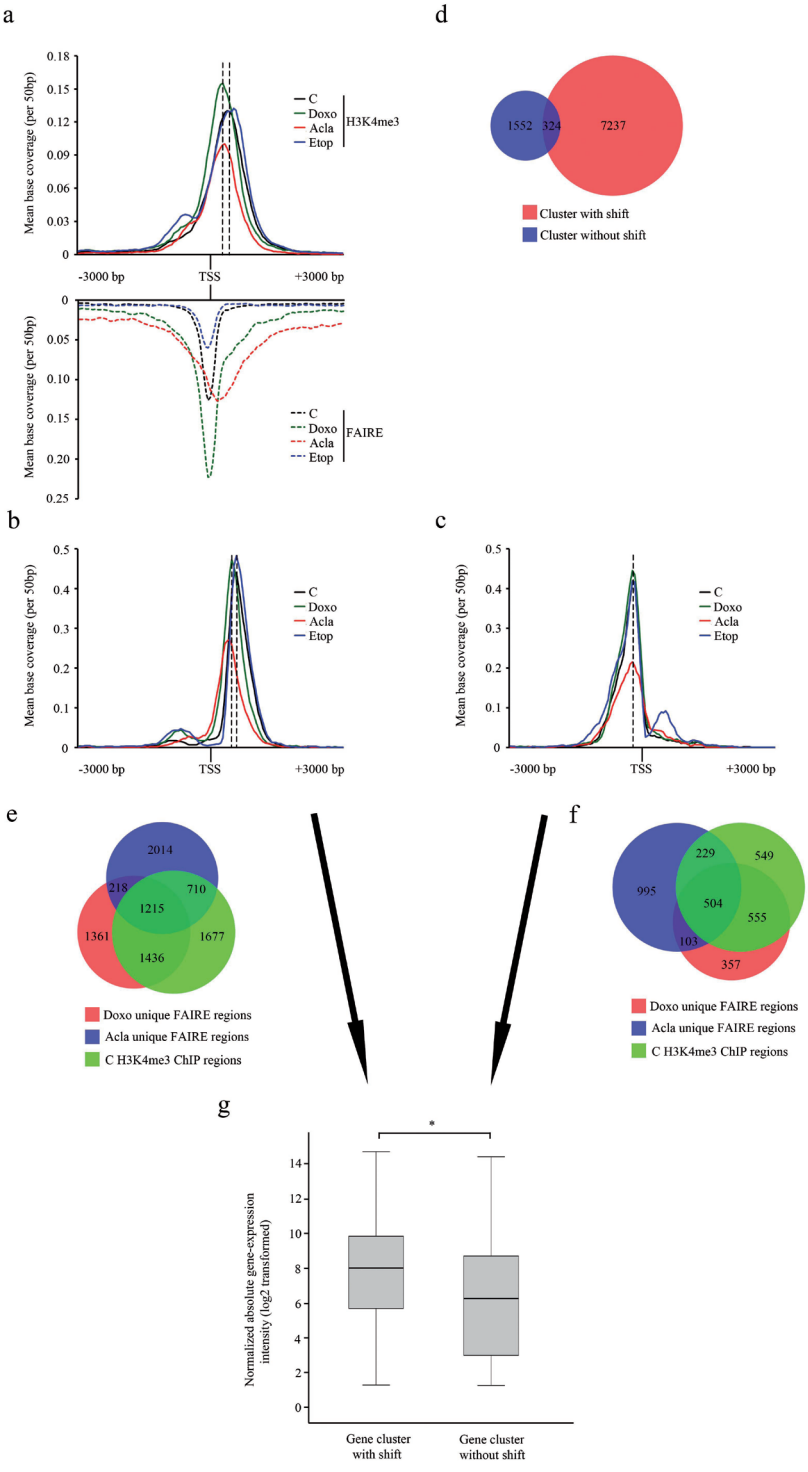
a
Mean base coverage (per 50bp)
0.18
0.15
0.12
0.09
0.06
0.03
0
C
Doxo
Acla
Etop
H3K4me3
-3000 bp
TSS
+3000 bp
0
0.05
0.10
0.15
0.20
0.25
FAIRE
d
1552
324
7237
Cluster with shift
Cluster without shift
b
c
e
2014
218
710
1215
1361
1677
1436
Doxo unique FAIRE regions
Acla unique FAIRE regions
C H3K4me3 ChIP regions
f
229
549
995
504
555
103
357
g
Normalized absolute gene-expression intensity (log2 transformed)
*
Gene cluster with shift
Gene cluster without shift

Figure 6. Doxo and Acla reposition histone H3K4me3 for active genes. (a) Distribution of H3K4me3 peak regions around TSS of MelJuSo cells 24 hrs post drug removal. MelJuSo cells were first incubated for 2 hrs with Doxo, Acla or Etop and fixed for ChIP-seq 24 hrs post drug removal. The ChIP-seq peak regions were aligned to a region of 3 kb up- and down-stream of the TSS of all RefSeq genes and the distribution was plotted (top panel). Bottom panel: the FAIRE-seq distribution at the same regions as shown in Figure 5e. Dotted vertical line indicates the position of the mean distribution of the H3K4me3 peak regions from Doxo, Acla versus Etop and untreated samples. **(b, c)** Sub-clustering of H3K4me3 ChIP-seq peak regions for all RefSeq genes from (a). The peak regions were separated into two clusters where the H3K4me3 mark was shifted (b) or not (c) relative to TSS. Cluster B shows genes where Doxo and Acla repositioned the H3K4me3 mark while this histone mark was not affected in untreated or Etop-treated cells. **(d)** Venn diagram showing the distance of TSS of the genes in sub-cluster regions (b) and (c) with a cut-off of 6 kb. Shared regions in the Venn diagram indicate genes that have their TSS within 6 kb. Venn diagram was generated as described in [70]. **(e, f)** Venn diagram showing the overlap between H3K4me3 ChIP-seq peak regions of untreated cells with Doxo- or Acla-induced FAIRE-seq peak regions. Analyzed were the regions in cluster (b) and (c) respectively. Venn diagram was generated as described in [70]. **(g)** Transcriptional activity of genes within the two sub-cluster regions before drug treatment. The expression values of genes from cluster (b) and (c) were extracted from Illumina microarray and a boxplot showing the expression of all genes in the respective clusters was generated. Student's t-test was used to calculate * *p*-value=3.15165E-77.

24 hrs or 6 days post-drug administration, various tissues were isolated for gene expression analyses. This experiment was performed in biological duplicate that yielded strongly reproducible sets of altered transcripts (Fig. 7a and Supplementary Fig. 28a). Three different effects were observed in mice. Firstly, Doxo and Etop did not alter the transcriptome of the lung (data not shown). Secondly, both Doxo and Etop deregulated a strongly overlapping set of genes in the liver, even after 6 days (Fig. 7a and Supplementary Fig. 28b). This suggests that the DDR response and detoxification pathways may be dominant in this organ (Supplementary Table 4). Thirdly, Doxo selectively altered the transcriptome of the heart. Altered transcription in the heart has recently been correlated to cardiotoxicity and associated with inhibition of TopoII by Doxo[38]. The transcriptome was altered at 24 hrs and restored 6 days post-application of Doxo and cannot be solely attributed to the DNA damage response, since no transcription changes were observed from Etop (Fig. 7a), despite the similar level of initial DDR (visualized by γ-H2AX staining) observed from both Doxo and Etop treatment (Supplementary Fig. 29a). Histology of heart specimens did not show any apoptosis, immune cell infiltration or other abnormalities resulting from the drug applications (Supplementary Fig. 29b), indicating that the altered transcriptome was a direct consequence of Doxo exposure of heart tissue.

Of note, Doxo strongly increased histone gene expression in the heart and liver of mice (Fig. 7b, Supplementary Fig. 28a and c), which usually occurs only during cell division[39]. Immuno-histochemistry did not reveal any dividing Ki-67 positive cells in the heart (Supplementary Fig. 29c), suggesting that histone expression is increased to compensate for the degradation of histones after eviction by Doxo rather than a response to cell division. In addition, when the genes differentially regulated in the heart by Doxo exposure were subjected to Ingenuity Pathway Analysis, a strong and significant enrichment of genes acting in *Tumoricidal Function of Hepatic Natural*

Killer Cells and *Interferon Signaling Pathways* was observed (Fig. 7c, Supplementary Table 4). Interferons can induce cardiotoxicity[40,41], possibly by inducing signaling pathways similar to those induced by Doxo.

To test whether Doxo also evicts histones from chromatin *in vivo*, mice were injected with Doxo or Etop, and 4 hrs post-drug administration, hearts were isolated for FAIRE-seq. Similar to the observations in cell lines, FAIRE-seq on heart tissue showed a higher enrichment of FAIRE peak regions (i.e. histone-free DNA fragments) around TSS after Doxo treatment unlike after Etop exposure (compare Fig. 7e with Fig. 5e). This suggests that Doxo not only induces a reproducible set of transcripts 24 hrs after injection, but also evicts histones from the same genomic areas. To investigate whether Doxo-induced histone eviction correlated to transcriptome changes in the heart, the FAIRE-seq data were integrated into the microarray results. Presence of Doxo-induced FAIRE-seq peak regions within the promoter regions or the gene bodies was observed for more than 70% of transcripts differentially altered in Doxo-treated heart (*p*-value=1.914E-26 related to the whole genome) (Fig. 7d, more genes in Supplementary Fig. 30), which is consistent with the observations in tissue culture cells.

Nonetheless, Doxo is primarily an anti-cancer drug, and to test the effect of Doxo on tumors in an *in vivo* setting, mice carrying a drug-sensitive BRCA1/p53-deficient mammary tumor were injected *iv* with a single dose of the drug. Subsequently, FAIRE-seq and microarray analyses were performed on the tumors following the same schedule as for the tissues. Doxo as well as Etop altered the transcriptome of the tumor, as some 60 genes were uniquely deregulated in tumors exposed to Doxo *in vivo*. In 30% of the altered transcripts, Doxo-induced FAIRE-seq peak regions were present within 3 kb of TSS or on the gene bodies of differentially expressed genes (Supplementary Fig. 31). Yet, similar to the results obtained from tissue culture cells and heart (Fig. 5e and 7e), higher enrichment of FAIRE-seq peak regions around the TSS was observed in tumor tissue of Doxo-treated mice than the control or Etop-treated mice, implicating histone eviction induced by Doxo (Fig. 7f).

Doxo-induced histone eviction delayed DNA repair (Fig. 3), which may contribute to better tumor elimination but also tissue toxicity *in vivo*. To visualize this, major tissues from the mouse experiments were subjected to immune-histochemistry against γ-H2AX. Whereas γ-H2AX was detected in both Doxo- and Etop-exposed tumors 4 hrs post exposure (Supplementary Fig. 29a), this DNA damage mark only prevailed in tumors from Doxo-treated mice 24 hrs later (Fig. 7g). It was also the case for other tissues tested (Supplementary Fig. 29a). Similar to the observations in tissue culture cells (Fig. 3e), Doxo attenuated the DNA damage response and led to persistent damage as well as DDR signaling *in vivo* as may be explained by histone eviction from the loose-structure chromosomal regions, as described above.

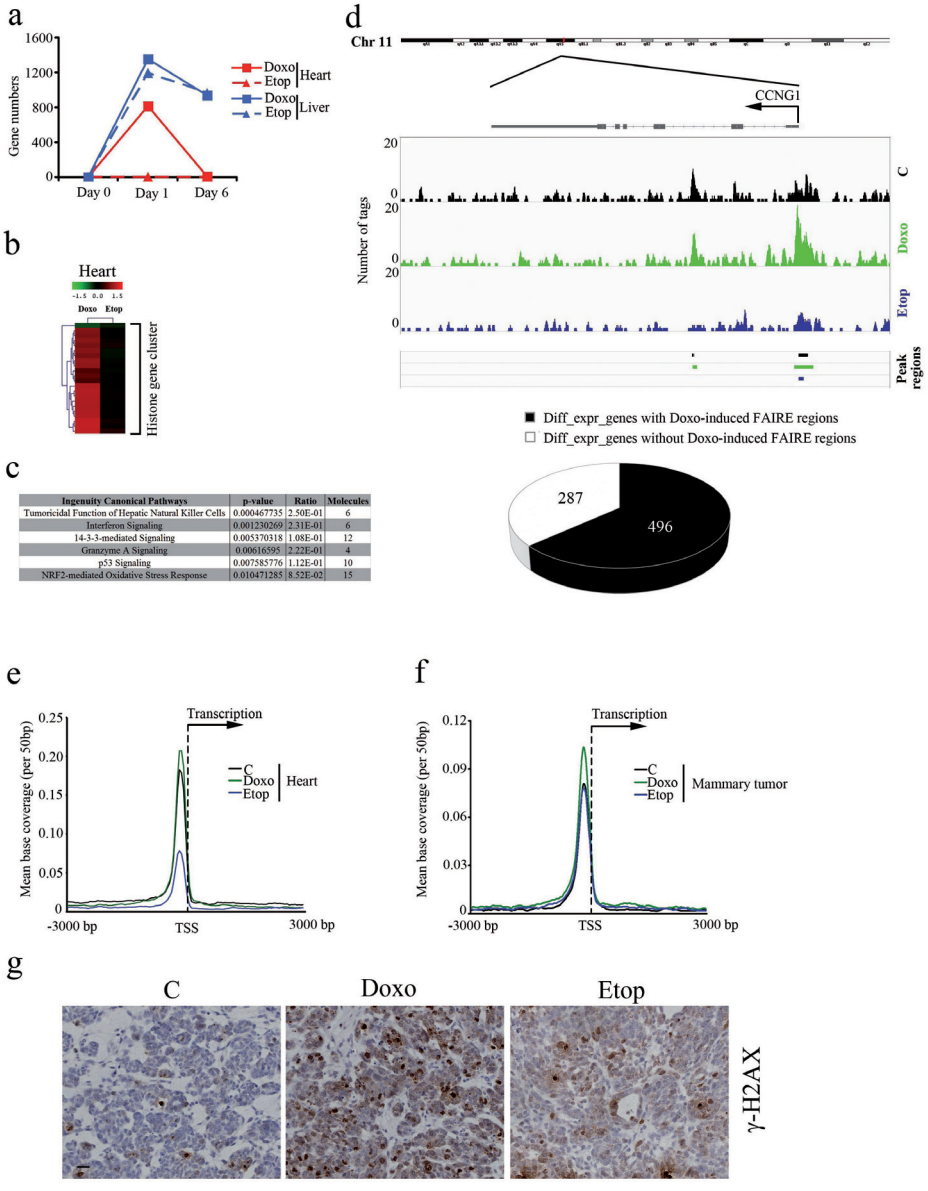

Ingenuity Canonical Pathways	p-value	Ratio	Molecules
Tumoricidal Function of Hepatic Natural Killer Cells	0.000467735	2.50E-01	6
Interferon Signaling	0.001230269	2.31E-01	6
14-3-3-mediated Signaling	0.005370318	1.08E-01	12
Granzyme A Signaling	0.00616595	2.22E-01	4
p53 Signaling	0.007585776	1.12E-01	10
NRF2-mediated Oxidative Stress Response	0.010471285	8.52E-02	15

Figure 7. *In vivo* responses to Doxo or Etop treatments. (a) Expression arrays were generated from livers or hearts of mice 1 day or 6 days after *iv* bolus injection of Doxo or Etop and compared to expression in respective organs from untreated mice. Significantly changed genes were calculated with linear models for microarray data (LIMMA), based on two mice per data point. **(b)** Heat map showing histone gene cluster expression in the hearts of Doxo- or Etop-treated mice related to control mice. Color indicates the log-fold change compared to control. **(c)** Enrichment of pathways from differentially regulated genes in the hearts 24 hrs post-Doxo treatment was determined by Ingenuity Systems Pathway Analysis. Shown are the most significant pathways. **(d)** Peak regions of FAIRE-seq from mouse hearts 4 hrs post-Doxo or Etop injection are compared to genes differentially regulated at 24 hrs after injection. Top: Illustration of FAIRE-seq reads as well as the peak regions of the gene CCNG1 for the three conditions.

TSS is indicated. Black area in the pie charts defines differentially expressed genes with Doxo-induced FAIRE peak regions (relative to control cells) within 3 kb upstream of the TSS or on the gene bodies. The new peak regions induced by Doxo exposure are indicated by arrows. **(e)** FAIRE-seq peak regions from the hearts of mice 4 hrs after Doxo exposure were enriched around TSS of all RefSeq genes in mice.

Anthracycline-induced histone eviction constitutes a major factor in initiating apoptosis of AML cells

To test the relevance of histone eviction induced by anthracyclines for human cancer, we selected a tumor type where samples can easily be obtained prior to and during treatment with anthracyclines. AML patients often have large numbers of circulating malignant cells (blasts) at diagnosis. Standard remission induction regimens consist of anthracyclines such as Daun and Ida followed by cytarabine, resulting in complete remission rates of over 70%[42]. Daun and Ida are Doxo variants and also induce histone eviction in MelJuSo/PAGFP cells (Supplementary Movie 5 and 6). AML blasts were isolated from patients before drug exposure and 2 hrs post *iv* bolus with Daun monotherapy, and immediately processed for FAIRE-seq analysis. A strong enrichment of FAIRE-seq peak regions surrounding the TSS regions was observed after Daun exposure (Fig. 8a), as also observed for cell lines and mouse tissues. This effect is illustrated for one gene (MS4A7) where histone eviction (in the form of more sequence reads) is shown in a region before the TSS (Fig. 8b; more genes, Supplementary Fig. 32). These results confirm the histone-eviction activity of anthracyclines in the most relevant clinical setting.

Anthracyclines such as Doxo, Daun or Ida have two different activities: DNA break formation and –as shown in this study– histone-eviction. To determine which activity is most relevant for driving tumors into apoptosis, we compared Doxo and Daun with Acla (that only induces histone eviction) and Etop (that only generates DNA breaks). MelJuSo cells were exposed to Doxo, Etop, Acla or Daun for 2 hrs, and then washed extensively before further culture. Cells were collected 18 or 24 hrs later and analyzed for apoptosis induction, as visualized by PARP cleavage. Doxo, Acla as well as Daun strongly induced apoptosis during this time course (Fig. 8c), unlike Etop, despite the initial stronger DNA damage and DDR signals induced by Etop (Fig. 3d and e). It should be noted that secondary strong induction of γ-H2AX was also observed for Doxo, Acla and Daun (Fig. 8c), which is a response to apoptosis initiation and execution resulting in DNA cleavage[43,44]. Freshly isolated AML blasts exposed *ex vivo* with the respective drugs showed identical results (Fig. 8e). In AML blasts, initial DNA damage response in terms of γ-H2AX was low with all treatments, possibly as a result of low TopoII expression in AML patients' blast cells[45,46]. We tested this by staining and comparing the expression level of TopoIIα between AML blasts and MelJuSo cells. No expression was observed in the isolated AML blasts, in contrast to the high level in MelJuSo cells (Fig. 8d). Free histone accumulation is assumed to be toxic to the cells[47,48]. It should be noted that Acla does not induce DNA damage but still induces strong cytotoxicity, and has been

used in some countries to treat AML effectively[49,50], which suggests that induction of histone eviction can be a more dominant factor for cytotoxicity of AML blasts. Collectively these data indicate that histone eviction by anthracyclines contribute strongly to cytoxicity of AML tumors. The additional effects on DDR, epigenetics and the transcriptome may further support anti-tumor effects with associated side effects.

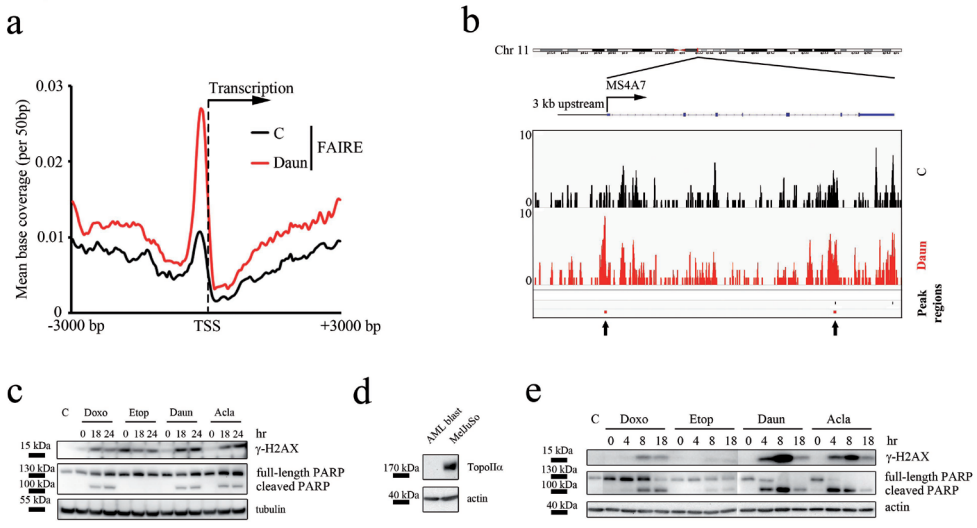

Figure 8. Histone eviction effect of anthracyclines on AML patients and blasts. (a) FAIRE-seq peak regions from blasts of an AML patient isolated before (black) and 2 hrs post (red) Daun infusion. All peak regions in a window of 3 kb around TSS of all RefSeq genes are shown. **(b)** Illustration of FAIRE-seq reads as well as the peak regions of the gene MS4A7 of AML blasts isolated before and 2 hours after completion of Daun infusion in an AML patient. The location of TSS and the 3 kb upstream region, as well as the intron and exon regions of the gene are indicated. The new peak regions induced by Daun exposure are indicated by arrows. **(c)** MelJuSo cells were exposed to 9μM Doxo, 60μM Etop, 10μM Daun or 10μM Acla for 2 hrs. Drugs were removed and cells were further cultured for the times indicated. Cells were lysed, separated by SDS-PAGE and WB was probed with the antibodies indicated. Tubulin is used as a loading control and positions of marker are indicated. The positions of PARP and the PARP cleavage product are indicated. C, untreated control. **(d)** MelJuSo cells and primary blast cells isolated freshly from AML patient were analyzed by WB to compare the level of TopoIIα. Actin is used as a loading control and position of marker proteins is indicated. **(e)** Primary blast cells isolated freshly from AML patient were exposed to 9μM Doxo, 60μM Etop, 10μM Daun or 10μM Acla for 2 hrs. Drugs were removed and cells were further cultured for the times indicated. Cells were lysed, separated by SDS-PAGE and WB was probed with the antibodies indicated. Actin is used as a loading control and positions of PARP, the PARP cleavage product and marker proteins are indicated. C, untreated control.

DISCUSSION

TopoII inhibitors like Doxo, Daun and Etop are broadly used in anti-cancer therapy. These inhibitors intercalate into DNA and then trap TopoII after DNA cleavage, thus generating DNA breaks and causing cell death. Yet, the anti-cancer effects of the inhibitors vary considerably in spite of their identical mode of inhibition.

The anthracyclines Doxo/Daun have a broader anti-tumor spectrum than Etop but may also induce more serious side effects, in particular cardiotoxicity. By using new technologies on "old" but broadly-used anti-cancer compounds, we discovered histone eviction from open chromatin as a novel mechanism of action of the anthracyclines. This effect is critical for apoptosis induction of primary AML cells.

How do anthracyclines Doxo/Daun evict histones from chromatin? We applied a Doxo variant, Acla that evicts histones yet does not induce DNA double-strand breaks. This and the observation that Etop fails to induce histone eviction uncouples DNA break formation from histone eviction. Chromatin remodeling and nucleosome repositioning constitute tightly regulated processes that require dedicated protein complexes fueled by energy expenditure[51]. It is therefore surprising that compounds like Doxo and Acla on their own can dissociate nucleosome structures without the need of energy. In an unambiguous *in vitro* setting employing reconstituted single nucleosomes (containing only histones and DNA), Doxo and Acla can still induce histone eviction and nucleosome dissociation upon intercalating into DNA. Doxo contains a tetracycline structure that intercalates into DNA and an amino sugar that then fills the DNA minor groove by interacting with DNA bases. Doxo-none that lacks the amino sugar fails to dissociate nucleosomes implying an important role of the sugar moiety. The reason became apparent when the location of the sugar moiety of Doxo was modeled into the nucleosome structure. The space taken by the sugar is normally occupied by histone side chains that stabilize chromatin structure. We propose that the intercalation of the tetracycline part of Doxo into DNA creates the energy for positioning the amino sugar properly to compete for space in the DNA minor groove at the cost of the histone side chains, resulting in histone eviction. Our data indicates that especially open and transcriptionally active chromatin is sensitive to histone eviction by the anthracyclines. Whether different chromatin states have their histone side chains differently positioned or whether they prevent entry of the drugs is unclear.

What are the consequences of histone eviction? We define two effects of histone eviction: attenuated DNA damage repair and epigenetic alterations. Doxo traps TopoII after the formation of DNA double-strand breaks to induce DNA breaks. One of the essential steps in the DDR cascade is the phosphorylation of histone variant H2AX that is also evicted by Doxo treatment. H2AX is then not phosphorylated (due to the absence of substrate around the DNA damaged sites), resulting in an attenuated DDR. This is in contrast with Etop, which fails to evict histones and allows H2AX phosphorylation and thereby swift DNA repair. As a result, Doxo treated cells or mouse tissues are characterized by markedly delayed DNA repair long after drug clearance. Signaling for apoptosis is then stretched which may contribute to the broader anti-cancer effects of Doxo than Etop in the clinic.

Eviction of modified histones could yield epigenetic changes, either following reintegration of marked histones or reinsertion of newly synthesized nascent histones.

As a result, the transcriptome will be affected, but in a surprisingly consistent manner. Independent repeats of microarray experiments of Doxo-exposed cells or mouse tissue showed a strongly overlapping set of genes being differently transcribed. Doxo apparently targets defined areas and genes, specified by open chromatin, for histone eviction. The empty space in the chromatin introduced by histone eviction could then provide freedom to nucleosomes to slide off of the remaining histone marks in the direction of the 'open space' in the chromatin (Fig. 6). It should be noted that the global shift of H3K4me3 in transcriptionally active genes after Doxo or Acla exposure is around 100 bp, which is in line with previous observations that nucleosome sliding occurs in that range [52]. The shift of nucleosomes and active histone mark H3K4me3 towards the TSS of active genes may affect the loading and moving of transcription factors, which relies not only on the proper histone marks but also the spacing to specific DNA sequences [53,54].

Histone eviction by Doxo and Acla correlates with transcriptional activity of genes, as shown in Fig. 5g and 6 and illustrated by the FAIRE-seq experiments. This is because transcriptionally active genes may pose a looser local chromatin structure. This has several consequences. Firstly, the DNA damage response, as detected by γ-H2AX (probably reflecting the site for DNA break formation as well) following TopoII inhibition by both Doxo and Etop, is almost exclusively observed for active rather than inactive genes. This cannot be explained by histone eviction (since the effect is also detected with Etop) but may reflect the activity of TopoII in supporting unwinding of DNA for transcription[55-57]. Secondly, it also implies that DNA breaks are not equally distributed over the genome in response to drug exposure. In combination with histone eviction, Doxo attenuates DNA repair at sites of open chromatin and transcriptional active genes, thus affecting transcription itself.

In vivo experiments reveal that tissues respond differently to Doxo. DNA repair is consistently delayed in Doxo-treated mice, as shown by persistent γ-H2AX staining in various tissues tested (Fig. 7g and Supplementary Fig. 22a). The DNA damage response dominates in the liver, whilst in the heart the histone eviction and consequent alterations in transcriptome are observed as an early response. An altered transcriptome in heart tissue is expected to correlate with Doxo-induced cardiotoxicity[38]. Although Etop also induces DNA damage in the heart (Supplementary Fig. 22a), it fails to alter the transcriptome. In the clinic, Etop-exposure is not associated with cardiotoxicity[58]. This suggests that, compared to other DNA damage inducing agents, additional effects due to Doxo-induced histone eviction could contribute to cardiotoxicity, including impaired DDR and DNA damage repair, persistent DNA damage signaling, and transcriptome changes. In addition, unlike Etop, Doxo selectively induced interferon-regulated genes in the heart. Such genes are normally suppressed by H3K9me2[59], which may be evicted and replaced in response to Doxo, thereby unleashing transcription. The organ-selective effects of Doxo may be due to different chromatin states, as compact chromatin prevents histone eviction. How chromatin states vary in different organs

is presently unclear. Still, the observed effects on the heart may contribute to Doxo-induced cardiotoxicity. Loss of histones and changes in chromatin structure also correlate with aging[60], and this process may be further accelerated in the hearts of Doxo-treated patients.

Why do anthracyclines have selectivity for cancer cells? In the classical interpretation, tumor cells are more sensitive to DNA breaks as they may cause mitotic catastrophe. Tumor cells have also been suggested to have higher expression of TopoII. However, AML blasts are highly sensitive to Daun and other anthracyclines, yet have varied (in our experiments undetectable) expression of TopoII[45,46]. Exposure of primary AML blasts to the various drugs used in this study showed that drugs that induce DNA breaks only (Etop) fail to induce apoptosis, unlike drugs enabling histone eviction (Acla). But why would histone eviction have some selectivity for tumors? Doxo and Acla evict histones preferentially in open transcriptionally active chromatin regions. Doxo may in fact sense transcriptionally active cells that usually correspond to more rapidly growing (tumor) cells. This may explain the therapeutic window for tumor tissue as well as some of the side effects. Among the drugs tested here, Acla is only used for a limited number of cancer types[50], though interestingly a genetic-modifying ability for this compound has been suggested[61], which may involve the histone-eviction effect. Etop is also commonly used for a restricted set of tumors[6], whilst Doxo has the broadest application in chemotherapy, perhaps by virtue of combining the activities of Etop and Acla. Doxo targets cells by inducing DNA damage and provoking histone eviction, resulting in epigenetic alterations and DDR delay of open-chromatin regions. As free histones are toxic to cells, in certain cases such as in AML treatment, anthracycline-induced histone eviction may exert more dominant cytotoxic effects. Indeed, Acla is used in the treatment of AML in some countries with strong anti-tumor effects[49,50]. We did observe strong toxicity of Acla both in tissue culture cells and primary AML blasts compared to Etop. The anthracyclines Daun, Ida and Acla are primarily used for intensive induction therapy of AML patients, which results in high remission rates[42]. Etop is only used for consolidation therapy[62] and did not improve remission and overall survival rates when used in remission induction schemes. This lack of additional activity of Etop may be explained by our findings[63]. These also highlight the different clinical efficacies of anthracyclines and Etop, and suggest that histone eviction induced by anthracyclines could play a major role in tumor elimination, as shown here with primary AML blasts.

The novel effect of anthracycline –histone eviction– and its consequences on DNA repair and epigenetics may have substantial effects in combination therapies where order and timing of drug application is of great importance. Indeed, correct sequential application of Doxo with EGFR inhibitors has a substantially stronger effect on eradication of breast tumors[64]. This was previously attributed to rewiring the apoptotic pathways, but could in fact be the consequence of delayed DNA

repair and transcriptional alterations due to histone eviction by Doxo. Sequential treatment with two drugs including an anthracycline may yield new and synergizing effects that could benefit cancer patients, based on the previously unknown properties of anthracyclines described here.

Drugs capable of selectively altering epigenetic codes have been sought for in the past decade[65], but it turns out that they have already been in use in the clinic as anti-cancer therapeutics for more than 40 years without realization.

METHODS

Constructs. Cloning of the various PAGFP histone variants is described in Supplementary Methods. All constructs were sequence verified. MelJuSo cells were stably transfected with the various histone constructs.

Microscopy. Cells expressing GFP, TopoIIα-GFP or PAGFP-labeled histones were analyzed by a Leica-AOBS system equipped with a climate chamber. Photoactivation was done with 405 nm laser light, image processing and calculation of released histones were performed as described before [15].

Immuno-histochemistry. Mouse tissues were formalin-fixed and processed by the animal pathology departments for H&E and γ-H2AX (Cell Signaling) staining. Tissue culture cells were fixed with cold methanol before staining with γ-H2AX antibody (Millipore) and DAPI, and analyzed by CLSM.

In vivo experiments. Mice were injected with 10 mg/kg of Doxo or 35 mg/kg of Etop *iv*. 4 or 24 hrs post-injection, tissues were collected and processed for FAIRE-seq, microarray analysis and pathology.

AML blasts isolation. AML blasts were isolated from the blood with BD Vacutainer CPT Cell Preparation Tube. Detailed description is in Supplementary Methods.

Experimental procedures. SDS-PAGE, Western blotting, nucleosome assembly and FAIRE-seq experiments were all performed as described in detail in Supplementary Methods.

Data analyses. The microarray data, FAIRE-seq and ChIP-seq data were processed by various programs[66-72] as described in detail in the Supplementary Methods. All data are available via Gene Expression Omnibus (GEO).

SUPPLEMENTARY INFORMATION

Supplementary Information includes extended methods, 6 movies, 24 figures, and 4 tables.

CONTRIBUTIONS

B.P. and J.N. designed and conceived the experiments. B.P. performed the cell biology and biochemical experiments with constructs made by L.J.. T.G. was instructive during initial experiments. X.Q. performed the FAIRE-Seq experiments and imaging quantification. A.V. and B.P. with help from W.Z. performed bioinformatics analysis. R.K. and M.N. performed sample preparation for next generation sequencing. O.v.T. and S.R. performed the drug studies in mice. P.H and J.J. provided AML patient materials. B.P. and J.N. wrote the manuscript with input from all authors.

ACKNOWLEDGEMENTS

We thank the Animal Pathology and NKI Mouse House Facility for helping with the *in vivo* experiments, and the NKI Central Genomics Facility for microarray and deep sequencing. We thank Lauran Oomen and Lenny Brocks from the NKI Digital Microscopy Facility, Anita Pfauth and Frank van Diepen of the NKI Flow Cytometry Facility for the technical support. We thank Jiying Song for the pathology analysis of mouse tissues, Wendy Sol for tumor implantation, Conchita Vens for the CFGE experiment, Coen Kuijl for image analysis software, Elisabetta Citterio and Joep Vissers for various antibodies and vectors, Massimiliano Maletta for structure modeling, Theo Knijnenburg for statistics support and Xiaole Shirley Liu (Harvard) for suggestions. We thank Ilana Berlin, Fred van Leeuwen, Piet Borst, Anton Berns, Sjoerd Rodenhuis, Hein te Reile and Bas van Steensel for support, critical discussions and reading of the manuscript. This work was supported by grants from the Netherlands Organization of Scientific Research NWO, Dutch Cancer Society KWF and an ERC Advanced Grant.

5

REFERENCES

1 Garnett, M. J. *et al.* Systematic identification of genomic markers of drug sensitivity in cancer cells. *Nature* **483**, 570-575 (2012).

2 Chapman, P. B. *et al.* Improved Survival with Vemurafenib in Melanoma with BRAF V600E Mutation. *New England Journal of Medicine* **364**, 2507-2516 (2011).

3 Farmer, H. *et al.* Targeting the DNA repair defect in BRCA mutant cells as a therapeutic strategy. *Nature* **434**, 917-921 (2005).

4 Bryant, H. E. *et al.* Specific killing of BRCA2-deficient tumours with inhibitors of poly(ADP-ribose) polymerase. *Nature* **434**, 913-917 (2005).

5 Arcamone, F. *et al.* Adriamycin, 14-hydroxydaimomycin, a new antitumor antibiotic from S. Peucetius var. caesius. *Biotechnology and Bioengineering* **11**, 1101-1110 (1969).

6 Hande, K. R. Clinical applications of anticancer drugs targeted to topoisomerase II. *Biochimica et Biophysica Acta (BBA) - Gene Structure and Expression* **1400**, 173-184 (1998).

7 Minotti, G., Menna, P., Salvatorelli, E., Cairo, G. & Gianni, L. Anthracyclines: Molecular Advances and Pharmacologic Developments in Antitumor Activity and Cardiotoxicity. *Pharmacological Reviews* **56**, 185-229 (2004).

8 Arcamone, F.-M. Fifty Years of Chemical Research at Farmitalia. *Chemistry – A European Journal* **15**, 7774-7791 (2009).

9 ClinicalTrials.gov. http://clinicaltrials.gov/ct2/results?term=doxorubicin+AND+adriamycin&recr=Open.

10 Nitiss, J. L. Targeting DNA topoisomerase II in cancer chemotherapy. *Nat Rev Cancer* **9**, 338-350 (2009).

11 Misteli, T. & Soutoglou, E. The emerging role of nuclear architecture in DNA repair and genome maintenance. *Nat Rev Mol Cell Biol* **10**, 243-254 (2009).

12 Gianni, L. *et al.* Anthracycline Cardiotoxicity: From Bench to Bedside. *Journal of Clinical Oncology* **26**, 3777-3784 (2008).

13 Tewey, K., Rowe, T., Yang, L., Halligan, B. & Liu, L. Adriamycin-induced DNA damage mediated by mammalian DNA topoisomerase II. *Science* **226**, 466-468 (1984).

14 Chen, G. L. *et al.* Nonintercalative antitumor drugs interfere with the breakage-reunion reaction of mammalian DNA topoisomerase II. *Journal of Biological Chemistry* **259**, 13560-13566 (1984).

15 Dantuma, N. P., Groothuis, T. A. M., Salomons, F. A. & Neefjes, J. A dynamic ubiquitin equilibrium couples proteasomal activity to chromatin remodeling. *The Journal of Cell Biology* **173**, 19-26 (2006).

16 Greene, R. F., Collins, J. M., Jenkins, J. F., Speyer, J. L. & Myers, C. E. Plasma Pharmacokinetics of Adriamycin and Adriamycinol: Implications for the Design of in Vitro Experiments and Treatment Protocols. *Cancer Research* **43**, 3417-3421 (1983).

17 Hande, K. R. *et al.* Pharmacokinetics of High-Dose Etoposide (VP-16-213) Administered to Cancer Patients. *Cancer Research* **44**, 379-382 (1984).

18 Schroeder, P. *et al.* Pharmacokinetics of etoposide in cancer patients treated with high-dose etoposide and with dexrazoxane (ICRF-187) as a rescue agent. *Cancer Chemotherapy and Pharmacology* **53**, 91-93 (2004).

19 DailyMed:Etoposide. http://dailymed.nlm.nih.gov/dailymed/lookup.cfm?setid=fd574e51-93fd-49df-92bc-481d0023505e.

20 Frederick, C. A. *et al.* Structural comparison of anticancer drug-DNA complexes: adriamycin and daunomycin. *Biochemistry* **29**, 2538-2549 (1990).

21 Luger, K., Mader, A. W., Richmond, R. K., Sargent, D. F. & Richmond, T. J. Crystal structure of the nucleosome core particle at 2.8[thinsp]A resolution. *Nature* **389**, 251-260 (1997).

22 Celeste, A. *et al.* Genomic Instability in Mice Lacking Histone H2AX. *Science* **296**, 922-927 (2002).

23 Stucki, M. *et al.* MDC1 Directly Binds Phosphorylated Histone H2AX to Regulate Cellular Responses to DNA Double-Strand Breaks. *Cell* **123**, 1213-1226 (2005).

24 Dong, Z., Zhong, Q. & Chen, P.-L. The Nijmegen Breakage Syndrome Protein Is Essential for Mre11 Phosphorylation upon DNA Damage. *Journal of Biological Chemistry* **274**, 19513-19516 (1999).

25 Neijenhuis, S. *et al.* Mechanism of cell killing after ionizing radiation by a dominant negative DNA polymerase beta. *DNA Repair* **8**, 336-346 (2009).

26 Binaschi, M. *et al.* Comparison of dna cleavage induced by etoposide and doxorubicin in two human small-cell lung cancer lines with different sensitivities to topoisomerase ii inhibitors. *International Journal of Cancer* **45**, 347-352 (1990).

27 Filion, G. J. *et al.* Systematic Protein Location Mapping Reveals Five Principal Chromatin Types in Drosophila Cells. *Cell* **143**, 212-224 (2010).

28 Ernst, J. *et al.* Mapping and analysis of chromatin state dynamics in nine human cell types. *Nature* **473**, 43-49 (2011).

29 Nakayama, J.-i., Rice, J. C., Strahl, B. D., Allis, C. D. & Grewal, S. I. S. Role of Histone H3 Lysine 9 Methylation in Epigenetic Control of Heterochromatin Assembly. *Science* **292**, 110-113 (2001).

30 Gaulton, K. J. *et al.* A map of open chromatin in human pancreatic islets. *Nat Genet* **42**, 255-259 (2010).

31 Hurtado, A., Holmes, K. A., Ross-Innes, C. S., Schmidt, D. & Carroll, J. S. FOXA1 is a key determinant of estrogen receptor function and endocrine response. *Nat Genet* **43**, 27-33 (2011).

32 Vermeulen, M. *et al.* Selective Anchoring of TFIID to Nucleosomes by Trimethylation of Histone H3 Lysine 4. *Cell* **131**, 58-69 (2007).

33 Guenther, M. G., Levine, S. S., Boyer, L. A., Jaenisch, R. & Young, R. A. A Chromatin Landmark and Transcription Initiation at Most Promoters in Human Cells. *Cell* **130**, 77-88 (2007).

34 Shan, K., Lincoff, A. M. & Young, J. B. Anthracycline-Induced Cardiotoxicity. *Annals of Internal Medicine* **125**, 47-58 (1996).

35 Creemers, E. E., Wilde, A. A. & Pinto, Y. M. Heart failure: advances through genomics. *Nat Rev Genet* **12**, 357-362 (2011).

36 Asperen, J. v., Tellingen, O. v., Tijssen, F., Schinkel, A. H. & Beijnen, J. H. Increased accumulation of doxorubicin and doxorubicinol in cardiac tissue of mice lacking mdr1a P-glycoprotein. *Br J Cancer* **79**, 108-113 (1998).

37 DailyMed:Doxorubicin. http://dailymed.nlm.nih.gov/dailymed/lookup.cfm?setid=5594d16e-72bf-4354-925e-c7591737ff1c

38 Zhang, S. *et al.* Identification of the molecular basis of doxorubicin-induced cardiotoxicity. *Nat Med* **18**, 1639-1642 (2012).

39 Ewen, M. E. Where the cell cycle and histones meet. *Genes & Development* **14**, 2265-2270 (2000).

40 Barry, S. P. & Townsend, P. A. in *International Review of Cell and Molecular Biology* Vol. 284 (ed W. Jeon Kwang) 113-179 (Academic Press, 2010).

41 Feenstra, J., Grobbee, D. E., Remme, W. J. & Stricker, B. H. C. Drug-induced heart failure. *Journal of the American College of Cardiology* **33**, 1152-1162 (1999).

42 Bennett, J. M. *et al.* Long-term survival in acute myeloid leukemia: the Eastern Cooperative Oncology Group experience. *Cancer* **80**, 2205-2209 (1997).

43 Rogakou, E. P., Nieves-Neira, W., Boon, C., Pommier, Y. & Bonner, W. M. Initiation of DNA Fragmentation during Apoptosis Induces Phosphorylation of H2AX Histone at Serine 139. *Journal of Biological Chemistry* **275**, 9390-9395 (2000).

44 Lu, C. *et al.* Cell Apoptosis: Requirement of H2AX in DNA Ladder Formation, but Not for the Activation of Caspase-3. *Molecular Cell* **23**, 121-132 (2006).

45 Gieseler, F. *et al.* Topoisomerase II activities in AML blasts and their correlation with cellular sensitivity to anthracyclines and epipodophyllotoxines. *Leukemia : official journal of the Leukemia Society of America, Leukemia Research Fund, U.K* **10 Suppl 3**, S46-S49 (1996).

46 Kaufmann, S. *et al.* Topoisomerase II levels and drug sensitivity in adult acute myelogenous leukemia. *Blood* **83**, 517-530 (1994).

47 Meeks-Wagner, D. & Hartwell, L. H. Normal stoichiometry of histone dimer sets is necessary for high fidelity of mitotic chromosome transmission. *Cell* **44**, 43-52 (1986).

48 Morillo-Huesca, M. *et al.* FACT Prevents the Accumulation of Free Histones Evicted from Transcribed Chromatin and a Subsequent Cell Cycle Delay in G1. *PLoS Genet* **6**, e1000964 (2010).

49 Hansen, O. P. *et al.* Aclarubicin plus cytosine arabinoside versus daunorubicin plus cytosine arabinoside in previously untreated patients with acute myeloid leukemia: a Danish national phase III trial. The Danish Society of Hematology Study Group on AML, Denmark. *Leukemia : official journal of the Leukemia Society of America, Leukemia Research Fund, U.K* **5**, 510-516 (1991).

50 Weiss, R. B. The anthracyclines: will we ever find a better doxorubicin? *Seminars in oncology* **19**, 670-686 (1992).

51 Hargreaves, D. C. & Crabtree, G. R. ATP-dependent chromatin remodeling: genetics, genomics and mechanisms. *Cell Res* **21**, 396-420 (2011).

52 Becker, P. B. Nucleosome sliding: facts and fiction. *EMBO J* **21**, 4749-4753 (2002).

53 Lemon, B. & Tjian, R. Orchestrated response: a symphony of transcription factors for gene control. *Genes & Development* **14**, 2551-2569 (2000).

54 Brogaard, K., Xi, L., Wang, J.-P. & Widom, J. A map of nucleosome positions in yeast at base-pair resolution. *Nature* **486**, 496-501 (2012).

55 Sperling, A. S., Jeong, K. S., Kitada, T. & Grunstein, M. Topoisomerase II binds nucleosome-free DNA and acts redundantly with topoisomerase I to enhance recruitment of RNA Pol II in budding yeast. *Proceedings of the National Academy of Sciences* **108**, 12693-12698 (2011).

56 Mondal, N. & Parvin, J. D. DNA topoisomerase II[alpha] is required for RNA polymerase II transcription on chromatin templates. *Nature* **413**, 435-438 (2001).

57 Ju, B.-G. *et al.* A Topoisomerase IIß-Mediated dsDNA Break Required for Regulated Transcription. *Science* **312**, 1798-1802 (2006).

58 Pai, V. B. & Nahata, M. C. Cardiotoxicity of Chemotherapeutic Agents: Incidence, Treatment and Prevention. *Drug Safety* **22**, 263-302 (2000).

59 Fang, T. C. *et al.* Histone H3 lysine 9 di-methylation as an epigenetic signature of the interferon response. *The Journal of Experimental Medicine* (2012).

60 Oberdoerffer, P. An age of fewer histones. *Nat Cell Biol* **12**, 1029-1031 (2010).

61 Andreassi, C. *et al.* Aclarubicin treatment restores SMN levels to cells derived from type I spinal muscular atrophy patients. *Human Molecular Genetics* **10**, 2841-2849 (2001).

62 Ding, L. *et al.* Clonal evolution in relapsed acute myeloid leukaemia revealed by whole-genome sequencing. *Nature* **481**, 506-510 (2012).

63 Bishop, J. F. *et al.* Etoposide in acute nonlymphocytic leukemia. Australian Leukemia Study Group. *Blood* **75**, 27-32 (1990).

64 Lee, Michael J. *et al.* Sequential Application of Anticancer Drugs Enhances Cell Death by Rewiring Apoptotic Signaling Networks. *Cell* **149**, 780-794 (2012).

65 Baylin, S. B. & Jones, P. A. A decade of exploring the cancer epigenome — biological and translational implications. *Nat Rev Cancer* **11**, 726-734 (2011).

66 Smyth, G. K. Linear Models and Empirical Bayes Methods for Assessing Differential Expression in Microarray Experiments. *Stat Appl Genet Mol Biol* **3**, Article 3 (2004).

67 Boyle, A. P., Guinney, J., Crawford, G. E. & Furey, T. S. F-Seq: a feature density estimator for high-throughput sequence tags. *Bioinformatics* **24**, 2537-2538 (2008).

68 Shin, H., Liu, T., Manrai, A. K. & Liu, X. S. CEAS: cis-regulatory element annotation system. *Bioinformatics* **25**, 2605-2606 (2009).

69 Blankenberg, D. *et al.* in *Current Protocols in Molecular Biology* (John Wiley & Sons, Inc., 2001).

70 Liu, T. *et al.* Cistrome: an integrative platform for transcriptional regulation studies. *Genome Biology* **12**, R83 (2011).

71 Zhang, Y. *et al.* Model-based Analysis of ChIP-Seq (MACS). *Genome Biology* **9**, 137 (2008).

72 Ye, T. *et al.* seqMINER: an integrated ChIP-seq data interpretation platform. *Nucleic Acids Research* **39**, e35 (2011).